

First-principles study of structural, vibrational and lattice dielectric properties of hafnium oxide

Xinyuan Zhao and David Vanderbilt

Department of Physics and Astronomy, Rutgers University, Piscataway, NJ 08854-8019
(February 25, 2002)

Crystalline structures, zone-center phonon modes, and the related dielectric response of the three low-pressure phases of HfO_2 have been investigated in density-functional theory using ultrasoft pseudopotentials and a plane-wave basis. The structures of low-pressure HfO_2 polymorphs are carefully studied with both the local-density approximation (LDA) and the generalized gradient approximation (GGA). The fully relaxed structures obtained with either exchange-correlation scheme agree reasonably well with experiment, although LDA yields better overall agreement. After calculating the Born effective charge tensors and the force-constant matrices by finite-difference methods, the lattice dielectric susceptibility tensors for the three HfO_2 phases are computed by decomposing the tensors into the contributions from individual infrared-active phonon modes.

PACS numbers: 77.22.-d, 61.66.-f, 63.20.-e, 77.84.Bw

Hafnia (HfO_2) is technologically important because of its extraordinary high bulk modulus, high melting point, and high chemical stability, as well as its high neutron absorption cross section. HfO_2 resembles its twin oxide, zirconia (ZrO_2), in many physical and chemical properties. The resemblance is attributable to the structural similarity between the two oxides, which can in turn be explained by the chemical similarity of Hf and Zr, which have similar atomic and ionic radii (i.e., ionic radii for Hf^{4+} and Zr^{4+} of 0.78 and 0.79 Å, respectively [1]) as a result of the so-called lanthanide contraction. Under ambient pressure, both oxides are monoclinic (m , space group $P2_1/c$) at low temperature, and transform to a tetragonal structure (t , space group $P4_2/nmc$) and then to a cubic structure (c , space group $Fm\bar{3}m$) as the temperature increases, as illustrated in Fig. 1.

High-K metal-oxide dielectrics have recently been the focus of substantial ongoing efforts directed toward finding a replacement for SiO_2 as the gate dielectric in complementary metal-oxide-semiconductor (CMOS) devices. HfO_2 , ZrO_2 and their SiO_2 mixtures show promise for this purpose [2,3]. Thus, a systematic theoretical investigation of the structural and dielectric properties of these dielectrics, in both bulk and thin-film form, is clearly desirable. As a first step in this direction, we have, in a previous paper [4], investigated the bulk structures and lattice dielectric response of ZrO_2 polymorphs. We found that the dielectric responses vary dramatically with the crystal phase. Specifically, we found that the monoclinic phase has a strongly anisotropic lattice dielectric tensor and a rather small orientationally-averaged dielectric constant owing to the fact that the mode effective charges associated with the softest modes are relatively weak.

This report presents the corresponding work on HfO_2 , providing the first thorough theoretical study of the structural, vibrational and lattice dielectric properties of the HfO_2 phases. Such properties are naturally expected to be similar to those of ZrO_2 in view of the chemical sim-

ilarities mentioned above. We find that this is generally true, although we also find some significant quantitative differences in some of the calculated properties.

The calculation of the lattice contributions to the static dielectric tensor ϵ_0 entails the computations of the Born effective charge tensors \mathbf{Z}^* and the force-constant matrices Φ . The \mathbf{Z}^* tensors, defined via $\Delta\mathbf{P} = (e/V) \sum_i \mathbf{Z}_i^* \cdot \Delta\mathbf{u}_i$, are obtained by finite differences of polarizations (\mathbf{P}) as various sublattice displacements (\mathbf{u}_i) are imposed, with the electronic part of the polarizations computed using the Berry-phase approach [5,6]. Here V is the volume of the unit cell, e is the electron charge, and i labels the atom in the unit cell. We then calculate the force-constant matrix, $\Phi_{ij}^{\alpha\beta} = -\partial F_i^\alpha / \partial u_j^\beta \simeq -\Delta F_i^\alpha / \Delta u_j^\beta$ by calculating all the Hellmann-Feynman forces F_i^α caused by making displacements u_j^β of each atom in each Cartesian direction in turn (Greek indices label the Cartesian coordinates). The resulting Φ matrix is symmetrized to clean up numerical errors, the dynamical matrix $D_{ij}^{\alpha\beta} = (M_i M_j)^{-1/2} \Phi_{ij}^{\alpha\beta}$ is constructed, and the latter is then diagonalized to obtain the eigenvalues ω_λ^2 and eigenvectors $\xi_{i,\lambda\beta}$.

The static dielectric tensor can be decomposed into a

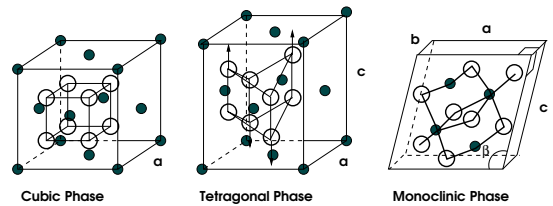


FIG. 1. Structures of the three HfO_2 phases. Small dark circles and larger open circles denote Hf and O atoms respectively. Hf-O bonds are only shown in m - HfO_2 . In t - HfO_2 , the arrows indicate the shift of oxygen pairs.

TABLE I. Calculated structural parameters for three HfO₂ phases using both LDA and GGA. Lattice parameters a , b , c are in Å, β is in degrees, and V (volume per formula) is in Å³. Internal coordinates x , y and z are dimensionless.

	Present LDA	Present GGA	Previous LDA ^a	Expt. ^b	ZrO ₂ LDA ^c
Cubic					
V	31.95	36.15	32.01	32.77	31.95
a	5.037	5.248	5.04	5.08	5.037
Tetragonal					
V	32.77	37.74	32.5		32.26
a	5.056	5.299	5.03		5.029
c	5.127	5.373	5.11		5.100
d_z	0.042	0.041	0.038		0.041
Monoclinic					
V	34.35	38.01	33.9	34.58	34.35
a	5.106	5.291	5.08	5.117	5.108
b	5.165	5.405	5.19	5.175	5.170
c	5.281	5.366	5.22	5.291	5.272
β	99.35	97.92	99.77	99.22	99.21
x_{Hf}	0.280	0.276	0.280	0.276	0.277
y_{Hf}	0.043	0.039	0.044	0.040	0.042
z_{Hf}	0.209	0.209	0.208	0.208	0.210
x_{O_1}	0.076	0.089	0.078	0.074	0.069
y_{O_1}	0.346	0.367	0.350	0.332	0.333
z_{O_1}	0.337	0.317	0.332	0.347	0.345
x_{O_2}	0.447	0.447	0.446	0.449	0.450
y_{O_2}	0.759	0.762	0.759	0.758	0.757
z_{O_2}	0.483	0.488	0.485	0.480	0.480

^aRef. [13].

^bRef. [12] for cubic; Ref. [11] for monoclinic.

^cRef. [4].

contribution ϵ_∞ arising from purely electronic screening, and the contributions of the IR-active phonon modes, according to [7]

$$\epsilon_{\alpha\beta}^0 = \epsilon_{\alpha\beta}^\infty + \frac{4\pi e^2}{M_0 V} \sum_{\lambda} \frac{\tilde{Z}_{\lambda\alpha}^* \tilde{Z}_{\lambda\beta}^*}{\omega_{\lambda}^2}. \quad (1)$$

Here the $\tilde{Z}_{\lambda\alpha}^* = \sum_{i\beta} Z_{i,\alpha\beta}^* (M_0/M_i)^{1/2} \xi_{i,\lambda\beta}$ are mode effective charges, e is the electron charge, M_0 is a reference mass that we take for convenience to be 1 amu, ω_{λ} is the frequency of the λ -th IR-active phonon mode, and V is the volume of the 3-atom, 6-atom, or 12-atom unit cell for cubic, tetragonal, or monoclinic cases, respectively. $\xi_{i,\lambda\beta}$, the eigendisplacement of atom i in phonon mode λ , is normalized according to $\sum_{i\alpha} \xi_{i,\lambda\alpha} \xi_{i,\lambda'\alpha} = \delta_{\lambda\lambda'}$.

The calculations are carried out within an ultrasoft pseudopotential [8] implementation of density-functional theory with a plane-wave basis and a conjugate-gradient minimization algorithm. The crystal structures of HfO₂ polymorphs are investigated in the local-density approximation (LDA) as parameterized by Ceperley and Alder [9] as well as in the generalized gradient approximation (GGA) using PBE parametrization [10]. We find that LDA yields slightly better agreement with the experi-

TABLE II. LDA dynamical effective charges \mathbf{Z}^* for HfO₂ phases. (Values in parentheses are GGA results.)

	Hf	O ₁	O ₂
Cubic			
	5.85	-2.93	-2.93
Tetragonal			
$x'x'$	5.84	-3.53	-2.31
$y'y'$	5.84	-2.31	-3.53
zz	5.00	-2.50	-2.50
Monoclinic			
xx	5.56 (5.57)	-3.09 (-3.10)	-2.48 (-2.47)
xy	-0.47 (-0.56)	0.97 (0.90)	0.20 (0.15)
xz	0.96 (0.91)	-0.58 (-0.53)	-0.39 (-0.36)
yx	-0.13 (-0.02)	1.37 (1.29)	0.21 (0.11)
yy	5.55 (5.57)	-2.73 (-2.70)	-2.82 (-2.87)
yz	0.14 (0.07)	-0.71 (-0.61)	0.35 (0.40)
zx	0.21 (0.27)	-0.18 (-0.20)	-0.07 (-0.09)
zy	0.41 (0.45)	-0.61 (-0.51)	0.43 (0.46)
zz	4.74 (4.64)	-2.24 (-2.16)	-2.58 (-2.52)

mental structures, and we therefore suggest that our LDA results for the dielectric properties are more reliable. The 4s and 4p semicore shells are included in the valence in the Hf pseudopotential, and an energy cutoff of 25 Ry is chosen. A 4×4×4 Monkhorst-Pack k-point mesh is found to provide sufficient precision in the calculations of total energies and forces, and a 4×4×20 k-point sampling is used for calculating the Berry-phase polarization [5]. Each atomic sublattice is displaced in turn along each Cartesian direction by ±0.2% in lattice units, the electronic polarization and Hellmann-Feynman forces are computed, and \mathbf{Z}^* and Φ , are then constructed by finite differences from the results.

Tabulated in Table I are the relaxed structural parameters for the three HfO₂ polymorphs, with the corresponding data for ZrO₂ listed in the last column for comparison [4]. While several structural determinations for *m*-HfO₂ can be found in the literature [1,11], corresponding results for the tetragonal and cubic phases are relatively sparse [12]. Nor has there been much theoretical work on hafnia; most important is the recent work of Ref. [13] which agrees quite well with our results. For *m*-HfO₂, the parameters given in Ref. [11] were used as the starting point of our relaxation procedures, while for *t*- and *c*-HfO₂ we started the relaxation from the zirconia experimental structures. It can readily be seen that both the LDA and GGA agree reasonably well with the previous work, but that the LDA yields a better overall agreement. Our total-energy calculations reproduce the correct energetic ordering of the phases (monoclinic then tetragonal then cubic) using either LDA or GGA.

Our results for the dynamical effective charges are presented in Table II. The symmetry of *c*-HfO₂ requires that \mathbf{Z}^* be isotropic on each atom. In *t*-HfO₂, the shifting of oxygen atoms creates two different configurations for oxygen atoms (denoted O₁ and O₂) and introduces off-diagonal elements. Thus, it is more natural to refer

TABLE III. Theoretical (LDA and GGA) and experimental (Ref. [15]) frequencies (in cm^{-1}) of Raman-active phonon modes in monoclinic HfO_2 .

Irrep	Mode	LDA	GGA	Expt. [15]
A_g	1	128	125	113
	2	142	132	133
	3	152	171	149
	4	261	248	256
	5	326	339	323 ^a
	6	423	382	382
	7	514	440	498
	8	608	557	577
	9	738	640	672
B_g	1	131	120	133
	2	175	152	164
	3	250	223	242
	4	380	318	336
	5	424	385	398
	6	533	466	520
	7	570	529	551
	8	667	627	640
	9	821	716	773 ^b

^aUnassigned.

^bRef. [17].

to a reference frame $x'-y'-z$ that is rotated 45° about the \hat{z} axis from the original Cartesian frame. $\mathbf{Z}^*(\text{O}_{1,2})$ become diagonal in this frame. In $m\text{-HfO}_2$, there are two non-equivalent oxygen sites (i.e., the 3-fold and 4-fold oxygens, labeled as O_1 and O_2 respectively). The crystal structure can then be regarded as composed of three kinds of atoms, namely, Zr, O_1 , and O_2 , which all have equally low symmetry, and their resulting \mathbf{Z}^* tensors are neither diagonal nor symmetric. The presence of two non-equivalent oxygen atoms with very different environments is reflected in the difference between the Born effective charge tensors for O_1 and O_2 . The anomalously large Z^* values indicate that there is a strong dynamic charge transfer along the Hf–O bond as the bond length varies, indicating a mixed ionic-covalent nature of the Hf–O bond. The resultant relatively delocalized distribution of the electronic charge is very similar to ZrO_2 , and is quite common in partially covalent oxides.

Since HfO_2 is isomorphic to ZrO_2 , the analysis of the phonon modes at Γ is the same for HfO_2 as for ZrO_2 [4]. Of 36 phonon modes predicted for $m\text{-HfO}_2$, 18 modes ($9A_g + 9B_g$) are Raman-active and 15 modes ($8A_u + 7B_u$) are IR-active, the remaining three modes being the zero-frequency translational modes. There are three IR-active modes (A_{2u} and two E_u) and three Raman-active modes (A_{1g} , B_{1g} and E_g) for $t\text{-HfO}_2$. Only one IR-active mode (one T_{1u} triplet) is predicted for $c\text{-HfO}_2$.

The Raman spectra of $m\text{-HfO}_2$ have been extensively measured experimentally [14–17], but the situation is not entirely satisfactory [16]. Issues concerning the number of modes and the mode assignments still remain unresolved, partially because of sample impurities and the broadness

TABLE IV. Frequencies ω_λ (cm^{-1}) and scalar mode effective charges \tilde{Z}_λ^* of IR-active phonon modes for HfO_2 phases, where $\tilde{Z}_\lambda^{*2} = \sum_\alpha \tilde{Z}_{\lambda\alpha}^{*2}$.

		LDA		GGA	
	Irrep	ω_λ	\tilde{Z}_λ^*	ω_λ	\tilde{Z}_λ^*
Cubic					
1	T_{1u}	286	1.12		
Tetragonal					
1	E_u	117	1.26		
2	A_{2u}	384	1.45		
3	E_u	536	1.13		
Monoclinic					
1	A_u	140	0.049	123	0.075
2	A_u	190	0.003	162	0.063
3	B_u	246	0.887	223	0.823
4	A_u	255	0.764	250	0.917
5	B_u	262	0.121	252	0.297
6	B_u	354	1.623	300	1.791
7	B_u	378	1.126	331	1.081
8	A_u	393	1.148	360	1.196
9	A_u	445	1.218	391	1.226
10	B_u	449	1.497	414	1.339
11	A_u	529	0.836	456	0.676
12	B_u	553	0.810	494	0.814
13	A_u	661	0.788	577	0.962
14	A_u	683	0.688	634	0.032
15	B_u	779	0.997	694	0.900

and weakness of some observed features. Thus, our *ab-initio* theoretical calculation can play an important role in establishing the Raman assignments. Table III shows the frequencies of the A_g and B_g Raman-active modes as calculated in LDA and GGA, together with the observed frequencies from a polarized Raman measurement on a high-quality single crystal [15]. The agreement is generally excellent; the observed Raman shifts mostly fall comfortably in the LDA–GGA range. A later single-crystal (but unpolarized) Raman spectrum [17] shows almost identical mode frequencies. However, a few details about the Table deserve comment. (i) We omit the weak mode reported as A_g at 268 cm^{-1} in Ref. [15] because it is not confirmed in Ref. [17] and it does not fit with our theoretical assignments. (ii) We assign the 323 cm^{-1} mode observed in Refs. [15,17] as A_g . (iii) The feature observed at 872 cm^{-1} in Ref. [15] is presumed to be a two-phonon process and is omitted. (iv) A weak mode is observed at 773 cm^{-1} in Ref. [17]; since this is consistent with our highest-frequency B_g mode, we assign it as such.

The frequencies of the IR-active phonon modes for the three HfO_2 phases are tabulated in Table IV, together with the scalar mode effective charges. It can be seen that the frequencies calculated in GGA are shifted to lower frequency by $\sim 10\text{--}16\%$ relative to the LDA ones, while the mode assignments coincide exactly. As indicated in Eq. (1), the contribution of a given IR-active mode to the

static dielectric constant scales as $\tilde{Z}^{*2}/\omega_\lambda^2$ [4], so that one or more low-frequency modes with large \tilde{Z}^* 's are needed to yield a large dielectric constant. As can be seen from Table IV, however, the few softest modes ($< 300 \text{ cm}^{-1}$) have relatively small \tilde{Z}^* 's, while the more active infrared modes come in the intermediate range of the IR spectrum ($350\text{--}450 \text{ cm}^{-1}$). The general pattern is very similar to the case of ZrO_2 .

The lattice contributions to the dielectric tensors are obtained by summing the second term of Eq. (1) over all the IR-active modes. Using the LDA we find

$$\epsilon_{\text{cubic}}^{\text{latt}} = \begin{pmatrix} 23.9 & 0 & 0 \\ 0 & 23.9 & 0 \\ 0 & 0 & 23.9 \end{pmatrix},$$

$$\epsilon_{\text{tetra}}^{\text{latt}} = \begin{pmatrix} 92.3 & 0 & 0 \\ 0 & 92.3 & 0 \\ 0 & 0 & 10.7 \end{pmatrix},$$

$$\epsilon_{\text{mono}}^{\text{latt}} = \begin{pmatrix} 13.1 & 0 & 1.82 \\ 0 & 10.8 & 0 \\ 1.82 & 0 & 7.53 \end{pmatrix}.$$

(The corresponding matrix elements of $\epsilon_{\text{mono}}^{\text{latt}}$ in the GGA tend to be larger than the LDA results by $\sim 18\%$.) When compared with ZrO_2 , the off-diagonal elements of $\epsilon_{\text{mono}}^{\text{latt}}$ are roughly doubled, while the diagonal elements become smaller. Most surprisingly, the x - y components of $\epsilon_{\text{tetra}}^{\text{latt}}$ become more than twice as large as for ZrO_2 , while the z component decreases by $\sim 28\%$. We find the isotropic $\epsilon_{\text{cubic}}^{\text{latt}}$ to be 23.9, somewhat smaller than the value of 31.8 for ZrO_2 [4].

A direct comparison of these dielectric tensors with experiment is not feasible since there are few experimental measurements, especially on the cubic and tetragonal phases. On the other hand, most measurements of which we are aware have been carried out on thin films (presumed to be monoclinic), and the reported dielectric constants span a wide range of 16–45 [3,18,19]. Assuming an isotropic $\epsilon_\infty \simeq 5$ [4], we obtained orientationally averaged static dielectric constants of 29, 70, and 16 (18 in GGA) for the cubic, tetragonal and monoclinic HfO_2 phases, respectively. Our results then agree reasonably well with the more recent results in Ref. [19] (thin film $\sim 1700 \text{ \AA}$) and Ref. [3] (ultrathin film $< 100 \text{ \AA}$) which report ϵ_0 to be 16 and 20 respectively. The surprising high ϵ_0 measured in other experiments could possibly be explained by the presence of $t\text{-HfO}_2$, which is known to be a metastable phase and which might be stabilized by film stress or grain-size effects [12,19,20].

In summary, we have investigated here the Born effective charge tensors, zone-centered phonons, and the lattice contributions to the static dielectric tensors for the three HfO_2 phases. It is found that the cubic and tetragonal phases have much larger dielectric response than the

monoclinic phase, with an even stronger anisotropy in $t\text{-HfO}_2$ than in $t\text{-ZrO}_2$. The overall dielectric constants for $c\text{-HfO}_2$ and $m\text{-HfO}_2$ are found to become smaller, while $t\text{-HfO}_2$ has a much greater dielectric constant, than the corresponding values in ZrO_2 . Moreover, our Raman results can be used in resolving the puzzles associated with the Raman spectrum for $m\text{-HfO}_2$.

This work has been supported by NSF Grant DMR-99-81193. We wish to thank E. Garfunkel for useful discussions.

-
- [1] R. Ruh and P. W. R. Corfield, J. Am. Ceram. Soc. **53**, 126 (1970).
 - [2] G. D. Wilk, R. M. Wallace, and J. M. Anthony, J. Appl. Phys. **89**, 5243 (2001).
 - [3] E. P. Gusev, E. Cartier, D. A. Buchanan, M. Gribelyuk, M. Copel, H. Okorn-Schmidt, and C. D'Emic, Microelectron. Eng. **59**, 341 (2001).
 - [4] X. Zhao and D. Vanderbilt, Phys. Rev. B. **65**, 075105 (2002).
 - [5] R. D. King-Smith and D. Vanderbilt, Phys. Rev. B **47**, 1651 (1993).
 - [6] R. Resta, M. Posternak, and A. Baldereschi, Phys. Rev. Lett. **70**, 1010 (1993).
 - [7] All three HfO_2 phases are non-piezoelectric, so the fixed-strain and free-stress dielectric tensors are identical for these systems.
 - [8] D. Vanderbilt, Phys. Rev. B **41**, 7892 (1990).
 - [9] D. M. Ceperley and B. J. Alder, Phys. Rev. Lett. **45**, 566 (1980).
 - [10] J. P. Perdew, K. Burke, and M. Ernzerhof, Phys. Rev. Lett. **77**, 3865 (1996); Y. Zhang and W. Yang, Phys. Rev. Lett. **80**, 890 (1998).
 - [11] J. Adam and M. D. Rodgers, Acta. Crystallogr. **12**, 951 (1959); R. E. Hann, P. R. Suttch, and J. L. Pentecost, J. Am. Ceram. Soc. **68**, C-285 (1985).
 - [12] J. Wang, H. P. Li, and R. Stivens, J. Mater. Sci. **27**, 5397 (1992).
 - [13] A. A. Demkov, Phys. Stat. Sol. (b) **226**, 57 (2001).
 - [14] E. Anastassakis, B. Papanicolaou, and I. M. Asher, J. Phys. Chem. Solids **36**, 667 (1975).
 - [15] H. Arashi, J. Am. Ceram. Soc. **75**, 844 (1992).
 - [16] C. Carlone, Phys. Rev. B **45**, 2079 (1992).
 - [17] A. Jayaraman, S. Y. Wang, S. K. Sharma, and L. C. Ming, Phys. Rev. B **48**, 9205 (1993).
 - [18] P. J. Harrop and D. S. Campell, Thin Solid films **2**, 273 (1968); M. Balog, M. Schieber, M. Michman, and S. Patai, J. Elec. Chem. Soc. **126**, 1203 (1979); C. T. Hsu, Y. K. Su, and M. Yokoyama, Jpn. J. Appl. Phys. **31**, 2501 (1992).
 - [19] K. Kukli, J. Ihanus, M. Ritala, and M. Leskela, Appl. Phys. Lett. **68**, 3737 (1996).
 - [20] R. C. Garvie, J. Phys. Chem. **82**, 218 (1978).